

Multi-Particle Correlation Observables in High-Energy
Nucleus-Nucleus Collisions*

R. Stock

Gesellschaft für Schwerionenforschung

D-6100, Darmstadt, West Germany

and

Nuclear Science Division

Lawrence Berkeley Laboratory

University of California

Berkeley, CA 94720

*Talk given at the Fifth High Energy Heavy Ion Study, Berkeley 1981



This work was supported by the Director, Office of Energy Research,
Division of Nuclear Physics of the Office of High Energy and Nuclear
Physics of the U.S. Department of Energy under Contract W-7405-ENG-48.

Multi-Particle Correlation Observables in High Energy

Nucleus-Nucleus Collisions

R. Stock

Gesellschaft für Schwerionenforschung

D-6100, Darmstadt, West Germany

and

Nuclear Science Division

Lawrence Berkeley Laboratory

University of California

Berkeley, CA 94720

I. Introduction

Studies of high energy nucleus-nucleus collisions have mostly focused on single particle inclusive measurements up to now¹⁾. The wide range of particle species in the final state, from nucleons, π , K, Λ to clusters and heavy nuclei, with their different specific energy ranges, required a set of devoted experiments exploiting the various specific messages such particles provide about the complicated overall process of a nucleus-nucleus collision. Multiplicity selection²⁾ and triggering on the extent of projectile degradation³⁾ have helped to study specifically peripheral and central collisions, thus removing in part the loss of information detail due to impact parameter averaging. In we describe the final state of N particles in the continuum by

$$O(\vec{p}_1 \dots \vec{p}_N) = |S(A_1, A_2, E, b; \vec{p}_1 \dots \vec{p}_N)|^2 t(\vec{p}_1 \dots \vec{p}_N) ,$$

where S is the matrix element for the flux into this configuration from a collision of nuclei A_1, A_2 at energy E/A and impact parameter b , and ρ is the appropriate phase space function, then we obtain single particle observables by taking the integral

$$\int O(\vec{p}_1 \dots \vec{p}_N) d\vec{p}_1 \dots d\vec{p}_{N-1} db = O(\vec{p}_N) .$$

It is clear that features of the reaction mechanism, as contained in S , will only in exceptional cases, as in remote regions of phase space, leave a distinct signature in this average. With N ranging up to $A_1 + A_2$ in central collisions, each event constitutes an ensemble average in this mode of observation, dominated by the phase space functional, which takes care of overall energy, momentum, and particle number conservation. Statistical models are naturally linked to such observables.

In order to obtain qualitatively different information, we want to study multiparticle exclusive observables, up to the extreme of a fully exclusive experiment identifying all the final state particles, including neutrals, leptons, and photons. The instrumentation effort is about linear with the number of particles per event, whereas the data analysis computer time grows nearly quadratically with N . This analysis, however, is now carried out event by event. From the N_i momenta obtained for each particle species i of the event, we shall construct certain collective variables, like the mean transverse and longitudinal momentum, overall momentum/energy flux directions, measures of symmetry and isotropy of the event, invariant mass spectra, etc. The high number of identical particles in each event provides some elementary statistics per event in this analysis, such that the total number of events required in order to satisfy statistical needs is not too high, thus keeping the overall

analysis effort within manageable limits. Consider the example of event-by-event analysis of $\langle p_{\perp}^2 \rangle / \langle p_{\parallel}^2 \rangle$. This ratio may be linked to the question of transparency in a nucleus-nucleus collision, measuring the overall degradation of the initial relative longitudinal motion of target and projectile nuclear matter. For complete thermalization we would expect $\frac{1}{2} \sum_i^N p_{i\perp}^2 \approx \frac{1}{2} \sum_i^N p_{i\parallel}^2$ for each event in its center-of-mass frame. The ratio of the two sums, taken event by event and then averaged over a set of events, is a more sensitive measure of equilibration than picking at random one particle out of each event (in a single particle inclusive measurement) and then constructing the same ratio where the sum is now taken over the number of events considered. The reason is that, in each event, equilibration takes momentum flux out of the longitudinal c.m. motion and puts it into transverse flux. This cannot be seen if only one particle is observed per event. Another simple example for the benefits of exclusive measurement is the analysis of two particle correlations. A double arm experiment gets one pair per event, whereas an exclusive measurement yields $N(N-1)/2$ pairs if N is the multiplicity per event of the particle species considered. With $N \approx 30$ protons in a central Ca + Ca collision³⁾, one event is equivalent in information to 435 double arm spectrometer events. Moreover, other types of observables may be constructed from the N exclusively measured protons.

The main purpose of this talk is, therefore, to consider the potential of exclusive measurements, a field that we are just beginning to get acquainted with in experiments like the streamer chamber^{3,4)}, the plastic ball⁵⁾, or emulsions⁶⁾. There are concepts of analysis available from particle physics, but we will have to find out which types of observables are of specific interest towards our understanding of nucleus-nucleus collisions.

After these introductory remarks, the structure of the talk will be as follows:

II. Global features of exclusively measured events:

- A. Number correlations, where we shall exploit the multiplicities of pions, protons, clusters, strange particles measured per event, as well as certain simple quantities as $\langle p_{\perp} \rangle$, $\langle p_{\parallel} \rangle$.
- B. Vector correlations, where we shall consider appropriate measures for isotropy, symmetries, clustering, or substructure in the final state like jets or preferred flux directions.

III. Hybrid analysis:

Here we consider the measurement of one or two specific fragments, like heavy spectator nuclei, high p_{\perp} particles, polarization of one particle, etc., along with a characterization of certain global features of the event such as a localization of the reaction plane or another anisotropy of the final state.

IV. Conclusions:

About future experiments employing the concepts developed, with a side glance at two-particle correlation studies.

II. Global features of exclusively measured events

How do we approach an exclusive measurement? Up to now, only charged particle exclusive observation has been employed in our field, using emulsions, the streamer chamber, and the Plastic Ball spectrometer. Simultaneous measurement of neutrals and photons will be a next significant step in the future⁷⁾. A streamer chamber picture³⁾ shown in fig. 1 for a central collision of $^{40}\text{Ar} + \text{KCl}$ at 1.8 GeV/A may serve

in order to illustrate the situation we encounter. We see about 40 charged particles, with negative and positive charge distinguished by curvature in the magnetic field and fast/slow particles identified by their ionization density in the chamber gas. Measuring of the tracks results in the picture of fig. 2 where we see a blind spot caused by a flare around the target. From three stereoscopic views measured for each event, track reconstruction in the magnetic field leads to a measurement of rigidity for each track. Combining rigidity, sign of curvature, and ionization density information, we proceed to an exclusive determination of charged particle identity and momentum/energy. Before we consider observables that may be associated with all these momentum vectors of each event, let us first look at certain simple types of analysis regarding multiplicities and mean values of momenta, event by event.

A. Number correlations

What we mean with such correlations is indicated in fig. 3. It shows event frequency contour lines in the plane of n^- multiplicity vs total charged particle multiplicity, for Ar + KCl at 1.8 GeV/A in the streamer chamber³⁾. The data are taken in a "minimum bias" trigger mode, registering each event in which there is no beam particle, $Z = 18$, detected within a 5° cone about the 0° direction, thus making sure that the projectile has undergone an interaction. The bulk of the cross section is found in peripheral interactions with small n_{π^-}, n_{ch} . Towards the more central collisions, nearly complete explosions into all the original single constituent charges, plus emission of more pions, is observed; the events approach the complete disintegration line along which $n_{ch} = Z_1^{Ar} + Z_2^{K,Cl} + n_{\pi^-} + n_{\pi^+}$ (where we assume $\langle n_{\pi^-} \rangle = \langle n_{\pi^+} \rangle$). The dashed line indicates the ridge of the cross section. The smooth

shift to higher n_{π^-} with increasing degree of disintegration indicates that there is no unusual pion production mechanism taking over in head-on collisions, at least not visibly at the multimillibarn level of cross sections to which this plot is sensitive. This disappoints the hopes of a phase transition setting in at small impact parameters when the reaction volume and the degree of momentum equilibration are large--at least as far as the idea of "copious pion production", originally associated with such a phase transition⁸⁾, is concerned. In fact, a closer analysis³⁾ shows that the mean number of π^- increases linearly with the number of participant nucleons.

However, we may not have chosen the interaction such that there is a chance to observe drastic signatures of a phase transition. First, with $A_1 = 40$, $A_2 = 37/39$ the reaction volume may still be too small. Furthermore, at 1.8 GeV/A the internal free energy per nucleon in central collisions may be too high, leading to an effective temperature that is far above the critical temperature associated, for example, with pion condensation. The high temperature, of about 100 MeV, is reflected in the close approach of the cross section ridge towards the complete disintegration line. The mean multiplicity of clusters with $Z \geq 2$ does not exceed one or two in the most violent events. It has been shown that the ratio of cluster to nucleon multiplicity can serve as a reaction thermometer⁹⁾.

Figure 3 also includes Λ production in this reaction¹⁰⁾, with the corresponding events given as dots in the contour diagram. The Λ particles were measured in a central trigger mode of the streamer chamber, which cuts out events with $n_{ch} \lesssim 25$, leaving the multiplicity contour lines unchanged at higher n_{ch} . We note that the Λ -producing events fall

mostly on the low n_{π^-} side of the cross section ridge. Λ particles emerge from associated production, $N + N \rightarrow \Lambda + K + N$ having the lowest threshold energy; rest mass and kinetic energy require about 1 GeV from the total available c.m. energy. Such events are, therefore, somewhat depleted in energy, resulting in less pion production. On the other hand, the nucleon "temperature" appears not to be decreased; the Λ events closely approach the complete disintegration limit. This aspect deserves further study when better Λ statistics become available.

It is obvious how rich in information such plots of rather simple results of an event-by-event analysis can be. Special "trigger" particle events, beyond Λ particles, may be studied this way, such as events with a high p_{\perp} particle, with several transverse clusters or with \bar{p} , $\bar{\Lambda}$ towards higher than Bevalac energies. Also, other variables may be used, like the total energy observed in π^- and π^+ vs the transverse energy of protons in each event, etc.

As a final example for number correlations, fig. 4 shows preliminary data for the sum of $|p_{\perp}|$ and $|p_{\parallel}|$ for the first 20 events of central Ar + KCl collisions¹¹⁾ at 1.8 GeV/A that have been completely analyzed. This analysis is quite time consuming at the present instrumentation level of measuring without computer automatization. The semiautomatic PEPR system at the University of Heidelberg is getting ready to take over this task; it will process about 5-10 full events per hour. In fig. 4, each event is represented in the c.m. system by a dot in the plane $\frac{2}{\pi N} \sum_i^N |p_{\perp}^i|$ vs $\frac{1}{N} \sum_i^N |p_{\parallel}^i|$. At these preliminary statistics, thermalization appears to be somewhat incomplete, but much less so than in cascade model predictions¹²⁾ that indicate a very high degree of transparency for this reaction at 1.8 GeV/A. The lower part of fig. 4 gives similar data for the reaction Ar + Pb at

800 MeV/A. We observe an almost isotropic distribution of momenta in the fireball center of mass.

B. Vector correlations

1. Visualizing complete events

Before we turn to a quantitative analysis of \vec{r} -space or \vec{p} -space global features of events, in terms of collective variables constructed from all the particle vectors, we may stop to consider which features we see, or expect to see, in nucleus-nucleus collision final states. Our expectations are mostly based on the recent discussion of participants, spectators, thermalization (isotropy in the c.m. system) versus transparency (elongation along the beam direction), cascades versus hydrodynamic flux (phase space statistics vs. sideways flow into certain preferred directions), etc. Can we identify such features in the confusing richness of information provided by the 50 to 100 vectors of each event? Can we guess about the appropriate observables? And finally, are there features obvious in the events that point towards other, new observables that might take us beyond the present horizon of models?

Let us proceed from the Ar + KCl "central" event shown in figs. 1 and 2. Figure 5 gives a side view of the momentum vectors in the lab frame, with x being the beam direction. Always remembering that we do not see the neutrals, carrying about half the momentum flux, we may still say the picture looks as expected; in a near-central collision of equal size nuclei, there is no target fragmentation region left, with particles rather slow in the lab frame. A thermalized system decaying (with high internal energy) in the overall c.m. frame would produce exactly the focusing into a 45° cone about 0° that we see. Figure 6 gives a "top" view but now in the c.m. frame. We think about momentum balancing, and

there appears to be some flux anisotropy. No leading particles are apparent. Figure 7, a side view, reveals an entirely different aspect of our event. It offers four jets, forward/backward and up/down, in a distinctly nonspherical pattern. Hydrodynamical prejudices: do we see target/projectile spectator flux because we did not really hit head-on, plus sideways splashing? Final view, fig. 8, in beam direction: the downward jet is still visible, but an obvious lack of p_{\perp} balancing reminds us of the missing neutrals and of all the various ways to be fooled by statistics in one single event.

What are the collective features? First, this event is flat; it stands upright in a plane made up by the x-z direction. Furthermore, it exhibits four jets, i.e. it is not even isotropic in that plane. Thus, we need a measure of flatness and of multi-jettiness. It is also clear from this sequence of views how rewarding it is to have a display capable of rotating the events into any desired orientation, in order to help our limited stereoscopic perception. An experimentalist's approach towards the collective observables would be to look at such displays of hundreds of events, but nobody has done this cheap, visual experiment yet.

Striking differences are obvious in comparing central events in Ca + Ca with Ca + Pb. Figures 9 and 10 show examples of these reactions at 1.8 GeV/A. The first exhibits a similar forward focus although the main part of the momentum flux seems to be diverted to the upper half plane, in which we also see a pair of π^- very close in momentum. Such two π^- correlations at $\Delta\vec{p} \rightarrow 0$, imbedded in the final state, exhibit the Hanbury-Brown, Twiss effect¹³⁾. Figure 10, Ca + Pb, looks qualitatively different, with about 30 rather slow particles covering all polar angles around the target, plus the forward cone of mostly fast particles.

Apparently, no common moving source is governing this pattern; do we see target "spectator" breakup plus a fireball? The incoming projectile energy is considerably degraded into transverse and even backward motion in the lab frame. In any moving frame, we expect this pattern to break up into two (or more) separate particle manifolds, calling for a collective analysis treating several superimposed flux patterns. Again, energy degradation is obvious in the Ca + Pb event shown in fig. 11, with no charged particle at all within about 15° to the beam axis. Whether or not this event is cylinder-symmetric and thus a candidate for near-zero impact parameter selection can only be seen in the 3-dimensional analysis.

From these pictures, we expect to need measures for substructure like clustering or jetting, for cylinder symmetry, for isotropy or flatness and, particularly in light projectile and heavy target reactions, for two separate components far separated in phase space. Furthermore, in semiperipheral reactions, we wish to localize the effective reaction plane between projectile fragments and recoiling target remnants.

2. Axes and scalar measures of event structure

In this section, we shall introduce the concepts of sphericity¹⁴⁾ and thrust¹⁵⁾ analysis, developed in particle physics. After looking at some applications to relativistic heavy ion reactions we shall be in the position to see their benefits and limitations in our case and to look out for other, more flexible pattern analysis methods, such as the minimum spanning tree¹⁶⁾.

Sphericity analysis

Here we are fitting a triaxial ellipsoidal shape to the square of the momentum components of the $i = 1 \dots N$ final state particles, in their c.m. frame; the method is formally identical to the inertia axis determination

of a rigid body, with the local mass density replaced by the local square momentum (scalar) density. The usefulness for identification of back-to-back jets in hadron or e^+e^- physics is obvious; the high momentum flux along the jet axes is accentuated by the p^2 weight, which suppresses the other reaction products that emerge from soft scattering.

Formally, one proceeds as follows:

Construct the quantity

$$S(\hat{n}) = 3 \frac{\sum_i^N p_{i\perp}^2}{\sqrt{2}} \frac{\sum_i^N p_i^2}{\sum_i^N p_i^2} ,$$

where \hat{n} is an arbitrary direction unit vector, and $p_{i\perp}^2$ is the component squared of the i th particle momentum perpendicular to \hat{n} . The axis of maximum elongation is the one of minimum inertia \approx flux perpendicular to this axis; therefore, the sphericity is obtained as

$$S = \text{Min}_{\hat{n}} S(\hat{n})$$

by variation of the direction \hat{n} . This is equivalent to finding the highest eigenvalue Q_3 and, in addition (for further information) the other two, Q_2 and Q_1 , of the symmetrical matrix

$$M_{\alpha\beta} = \sum_i^N p_{i\alpha} p_{i\beta}, \quad i = 1 \dots N, \alpha, \beta = 1 \dots 3 .$$

Normalizing $Q_1 + Q_2 + Q_3 = 1$, and ordering $0 \leq Q_1 \leq Q_2 \leq Q_3$, we can express the sphericity by

$$S = \frac{3}{2}(Q_1 + Q_2) \begin{cases} \rightarrow 0 \text{ for } Q_3 \gg Q_1, Q_2, \text{ i.e. a "two jet-pencil"} \\ \rightarrow 1 \text{ for } Q_1 \approx Q_2 \approx Q_3, \text{ i.e. a sphere.} \end{cases}$$

If $Q_1 \approx Q_2$ we have a rotation ellipsoid, but if $Q_1 \ll Q_2$ the event is flat. We thus define

$$\text{Flatness } F = \frac{\sqrt{3}}{2}(Q_2 - Q_1) \left\{ \begin{array}{l} \rightarrow 0 \text{ for cylinder symmetry} \\ \text{about } Q_3\text{-direction} \\ \rightarrow \frac{S}{\sqrt{3}} \text{ for coplanar events.} \end{array} \right.$$

The coplanarity is a characteristic feature of e^+e^- , 3-jet events where the third jet results from gluon bremsstrahlung.

What we do in sphericity analysis is to fit a four-parameter collective flux ellipsoid (Q_1, Q_2, Q_3 , direction of Q_3) to the square of the N momenta of each event. It is clear that N has to be large in order to attach significance to four variables; we shall illustrate this below. Furthermore, in the application to nucleus-nucleus collisions we have to avoid being misled by the square-momentum analysis; one heavy projectile or target fragment with its high p in the c.m. is sufficient to dominate all the other particles, pulling the Q_3 direction along with it. Therefore, sphericity is very sensitive to spectator motion. The positive aspect of this: if we search for the reaction plane of a semiperipheral reaction, $S(\hat{n})$ is the appropriate measure to select it from an isotropic participant background.

Thrust analysis

Here we simply look at momentum flux density. The quantity

$$T(\hat{n}) = \frac{\sum_i^N |\vec{p}_i \cdot \hat{n}|}{\sum_i^N |p_i|}, \quad \hat{n} \text{ arbitrary direction unit vector,}$$

may be visualized as the flux density in direction \hat{n} , as given by a scalar, which we may take as the radius in \hat{n} direction of a deformed flux spheroid. The direction of maximum elongation is called thrust direction, and

$$T = \text{Max}_{\hat{n}} T(\hat{n}) \begin{cases} + 1 \text{ for 2 jets back to back along } \hat{n} \\ + \frac{1}{2} \text{ for isotropic emission} \end{cases}$$

is defined as the (maximum) thrust of an event.

Thrust analysis determines just one scalar plus a direction, as the collective features of the event. Clusters that are "coalesced" out of nucleons are given the same weight in T as their constituents would have. On the other hand, one axis may not be sufficient in all cases of interest. We might then want to construct the whole $T(\hat{n})$ flux spheroid and fit certain simple shapes to it (pancakes, cigars, etc.).

3. Applications of sphericity and thrust analysis

a. Negative pion emission in Ar + KCl at 1.8 GeV/A

We shall illustrate sphericity analysis in an application to π^- emission in central Ar + KCl events studied in the streamer chamber¹¹⁾. At 1.8 GeV/A, the mean π^- multiplicity is about 6 and the mean participant proton number is 30, indicating a selection of impact parameters $b \lesssim 0.3 b_{max}$ in this trigger mode³⁾.

Figure 12 gives a contour plot in p_L and rapidity y_{CM} of the invariant pion cross section, for all π^- from an analyzed sample of about 2000 events. The contours are approximately symmetric about midrapidity, with a slight shift towards positive rapidity caused probably by the fact that $A = 40$ collides with $A = 38$ and by the neutron excess of the projectile (π^- are produced by $n + N \rightarrow \pi^- + p + N$). So the pion source is moving with about the velocity of the $N + N$ center of mass. Emission is not quite isotropic, however, as can be seen from the dashed lines representing an isotropic source at midrapidity; there is a forward-backward enhancement of the yield. The same feature is obvious

from fig. 13, showing the distribution in cosine of observed emission angles in the c.m. system. We might conclude that there is in the c.m. system a memory of the beam direction preserved in the nucleon motion, i.e. that participant nucleons are not completely thermalized, because then the known forward-backward enhancement of π emission in nucleon-nucleon collisions would explain our observation. However, this conclusion is not stringent from the data of figs. 12 and 13 for the following reasons:

1. Due to the finite number of nucleons in the colliding nuclei, there may occur a shift away from midrapidity in the effective center of mass of each individual event, caused by fluctuation in the projectile and target participant numbers. The individual c.m. rapidities would be symmetrically distributed about midrapidity, and a half-width $\Delta y \approx 0.3$ would be sufficient to explain the elongation of the contour plot along $\pm y$. We would, therefore, like to see whether this elongation is a feature of the individual events or one of ensemble averaging.
2. As to fig. 13, it is not so much the emission angle but the momentum flux angular distribution of the pions that we should analyze.

This appears to be a good case for sphericity analysis. There are no leading, high \vec{p} pions that might obscure the picture. Figure 14 gives the angular distribution for the direction of the main axis, Q_3 , resulting from a fit of all events with $n_T \geq 4$. We note here, without proof, that the direction of Q_3 is the most statistically significant of the four sphericity analysis parameters, i.e. the most reliable in a situation of relatively small event multiplicity. The corresponding Monte Carlo simulation gives a flat distribution. We can now safely conclude that the square momentum flux in π^- shows a forward-backward enhancement on the event-by-event basis.

Proceeding to the other collective parameters, fig. 15 shows event frequency contours in the plane of coplanarity or flatness vs sphericity. The events cluster at $F \approx 0.2$ and $S \approx 0.5$, i.e. at drastically nonspherical, rather flat shapes. Figure 16 shows the projection onto the S axis; the length of the main axis appears to be about twice that of the other axes. The events thus look like flattened cigars, oriented preferentially along the beam axis. But comparing with a Monte Carlo simulation with respect to S and F leads to a big surprise! Figure 17 shows this for S, giving the ratio of true event to Monte Carlo event frequency along the S axis; the ratio is compatible with 1 for all S, within statistics. The same is found for the flatness variable. At the level of statistics provided by several thousand events and with a mean particle multiplicity of about 8 (resulting from the cut $m_{\pi} \geq 4$), the parameters S and F are governed by finite particle number effects; i.e., a multiplicity 8 event, under the square weighting of momenta, is on the average nonspherical by its very nature!. The full set of collective parameters, introduced by sphericity analysis, thus over-stretches the information that 8 momentum vectors can provide. We need more particles in order to make the square momentum flux density functional continuous enough for the fit not to get hooked on statistical fluctuations.

We conclude that the elongation direction is the least critical parameter in sphericity analysis, which makes a maximum thrust analysis the more promising candidate in such low M cases because it focuses specifically on this feature of the event. Much better event statistics may help for the essay about S and F, with some small signal standing out above the Monte Carlo simulation.

At the present level of analysis, we may conclude that π^- emission is enhanced forward-backward in central Ar + KCl collisions at 1.8 GeV/A; but we cannot learn more about the collective features of the square momentum flux pattern.

b. Collective observables of proton emission, predicted by cascade and hydrodynamical models

After having absorbed the warnings about sufficiently high particle multiplicities from the pion case, let us turn to proton emission analysis from central collisions where the mean multiplicities are about 5 to 10 times larger. The analysis of experiments, like the streamer chamber or the plastic ball, will be progressing within the next year. Meanwhile, we may look at the predictions of the two most contradictory models for the reaction mechanism, cascades^{12,17)}, and hydrodynamics^{18,19)}.

The main difference in the predictions of these two models for central collisions of $A \approx 40$ nuclei is appropriately expressed in momentum flux variables; cascades predict drastic transparency effects towards the top Bevalac energies, i.e. $\langle p_{\parallel} \rangle > \langle p_{\perp} \rangle$ in the c.m. frame, whereas hydrodynamics predicts a 90° deflection of the incident momentum flux. Thus the cascade final state is a cigar along the beam direction, but hydrodynamical models predict a pancake momentum pattern, perpendicular to the beam axis at small impact parameters.

In terms of sphericity analysis, fig. 18 illustrates the cascade model predictions¹⁷⁾ for proton emission from $^{38}\text{Ar} + ^{38}\text{Ar}$ at 360 MeV/A and 1180 MeV/A. The variables used here are (1-sphericity), which we might call elongation, and the polar angle of the main axis Q_3 with respect to the beam direction. The plots refer to the c.m. frame, giving contour lines of event frequency in the (1 - s) vs Q_3 plane. Only

participant protons are included in the analysis of each event, i.e. those protons that did engage in the cascade. We are thus avoiding spectator effects; but note that these figures are not directly comparable to data except for the limiting ideal case of an extremely strict $b = 0$ selection in the data. Nevertheless, they may serve to enhance the specific features of cascade model predictions. For each energy, contours equivalent to an inelastic and central trigger mode are obtained by multiplicity cuts. At 360 MeV/A, the plot for $M \geq 4$ is again governed by small particle number effects; for $M \geq 20$ we observe shapes that are very close to perfect spheres: no transparency in central collisions at this energy but also no signal of a sideways enhancement ($\theta \rightarrow 90^\circ$). At 1180 MeV/A the picture is different. In the $M \geq 30$ selection we observe a statistically significant elongation, corresponding to a ratio of about 1.6:1 of the principal axis to the mean of the two smaller axes. The orientation is along the beam axis.

The cascade model thus predicts the onset of transparency in central Ar + Ar collisions already at intermediate Bevalac energies. Comparing with the $\{p_\perp\}$ vs $\{p_\parallel\}$ plot of the Ar + KCl data in fig. 4 we conclude, with the necessary reservations in view of very low statistics, that even at 1.8 GeV/A no such drastic transparency is observed. Note, moreover, that the data should be even more forward-backward enhanced because they still include some spectator motion (in the sense of the cascade model) due to the contributions from $b \neq 0$.

Turning to the hydrodynamical model, fig. 19 shows¹⁹⁾ the familiar plot of density time development in configuration space for a symmetric collision at 400 MeV/A. The three typical impact parameters range from peripheral to head-on. There are no spectators in hydrodynamics because

the collective pressure gradient, built up in the zone of geometrical overlap, acts on all the nucleons. The final state exhibits a collective sideways deflection ("bounce-off") of the momentum flow, increasing with smaller impact parameter. At $b = 0$, the final state is a pancake both in configuration and momentum space because $\theta = 90^\circ$ is the preferred flow direction, and we have cylinder symmetry about the beam axis. Figure 20 shows the result of a thrust analysis of these calculations, as a function of impact parameter b/b_{\max} . The lower horizontal axis gives the "bounce-off" angle θ , identical to the thrust direction, corresponding to the impact parameter shown on the upper horizontal axis. The maximum value of T decreases from complete elongation of the flux pattern along the beam direction for grazing collisions, to "isotropy" for head-on collisions. Here we observe an inadequacy of thrust analysis; it cannot, in the value of T , distinguish between a sphere and a cylinder symmetric but flat distribution. Generalized sphericity analysis, with its higher number of collective variables, could appropriately describe this final state: $Q_3 < Q_2 = Q_1$, $\theta(Q_3) = 0^\circ$.

We have to wait for more data analysis to decide how nature falls in between these two model extremes. There is one point important about these models: hydrodynamical predictions are A -invariant, whereas cascade predictions are not; at fixed incident energy, the cascade final state gets more spherical with increasing A . For heavy nuclei, the hydrodynamical approach appears to be more appropriate than for $A \lesssim 40$; we shall at Bevalac energies be trying to decide whether a slightly cigar-shaped cascade or a pancake hydrodynamical final state fits the data. The transient state of maximum compression, to which we have not yet found a direct experimental access, looks alike in both models (pancake shape in \vec{r} -space). Figure 21 summarizes these features in a schematic way.

4. More general pattern analysis

We have seen that event-by-event analysis of momentum thrust and sphericity appears appropriate, most of all, in collisions of equal mass nuclei, in order to select more sharply for $b \approx 0$ events [cylinder symmetry: $Q_1 = Q_2$, $Q_3 = 0$] and then check transparency/equilibration, and to decide between various models of the reaction dynamics by means of their characteristic flux predictions. However, the Ca + Pb events shown in figs. 10 and 11 indicated a problem not easily handled by thrust and sphericity; two or more separate components in the final state, perhaps to be identified with the spectator and participant regions of phase space, call for a more flexible treatment capable of identifying the particle "families" and then analyzing each one by itself. Furthermore, there may be other observable multiparticle correlation features, beyond our present concepts of equilibrium, cascades vs hydrodynamical flux, etc. Such features may be discovered by looking at other representations of the final state.

As an example for an \vec{r} -space representation that may be useful, fig. 22 shows a polar plot of the emission angles θ, ψ in the c.m. system, for all charged particles of a central Ar + KCl event at 1.8 GeV/A. A similar plot could be made separately for each kind of particle, found with sufficiently high multiplicity in the event, like all pions vs protons vs d, t, He. Clustering in configuration space would show up as regions of high point density. A pattern analysis method appropriate to such a "family" search is the minimum spanning tree¹⁶⁾, illustrated in fig. 23. Three families of particles are shown in a plane that could be that of the fig. 22 graph or any other suitable \vec{r} or \vec{p} space, 2- or 3-dimensional representation of the event. The quantity minimized is the

total length of lines connecting all the particles; the families thus emerge as branches with internal short distances, connected to a "tree" by a minimum number of long lines. The method is applicable to any kind of multi-axial, multicluster features, where the meaning of the axes depends on the choice of metric and representation. In 3-dimensional \vec{p} space, for example, this picture would be interpreted as a 3-jet event, and we might then look at the total momentum of each jet and obtain the mean p_{\perp} within each family with respect to its jet axis. In 3-dimensional \vec{r} space, we might check with the same method whether or not there is a preferred orientation of pion emission with respect to proton emission or whether there are participant and target/projectile spectator families. The resulting main branches would then fix the orientation of the impact plane. These examples may be sufficient to illustrate how the desired observable is connected to an appropriate choice of the metric in this method of analysis.

5. Experimental considerations

We have seen that collective analysis, event by event, may become meaningful provided that certain conditions are met:

- a. Multiplicities should be high for each family of particles, to be separately studied in the final state.
- b. The fraction of unobserved or misidentified particles should be kept as low as possible.
- c. The experiment should have a highly uniform detection efficiency over all 4π .

As to the multiplicities required, the sphericity analysis example of π^- from $\text{Ar} + \text{KCl}$ has served as a warning about finite particle number effects. In order for a collective degree of freedom (such as flatness)

to be a meaningful concept, there has to be a sufficient number of microscopic degrees of freedom (like single particle momenta) folding into its definition. Each event has thus to provide elementary statistics. The number of events considered can only in part make up for a lack of elementary statistics; it is obvious that even a million events, with two pions in each of them, cannot support a sphericity analysis. Requiring at least one order of magnitude in the ratio of microscopic to collective degrees of freedom, the mean number of about 40 charged particles in a central Ar + KCl collision may be just about sufficient to perform a 4-parameter sphericity analysis. We thus need all their individual momenta, and the experiment should have sufficient spatial resolution in order to register them. Track detectors and the streamer chamber are adequate in this respect. A multisegmented hodoscope array or a plastic ball type system must have a resolution of 2-4 degrees in both θ and ψ , which leads to the about 900 modules in the plastic ball/wall⁵⁾, as sketched in fig. 24.

At the extremes of attainable Bevalac reaction multiplicities, such as $\langle m_{ch} \rangle \approx 160$ in central Pb + Pb at 1 GeV/A, we may reach a critical point because neither of the familiar experiments will be fully adequate. How shall we go beyond? A general idea might be to give up individual particle identification, from which then to construct the collective observables, measuring local averages of certain particle, momentum or charge fluxes instead. The appropriate ways of calorimetry have not yet been worked out; the energy range of particles, from about 20 to 1000 MeV, mostly not yet minimum ionizing, is inconvenient. Particle physics calorimetry is not applicable in a straightforward manner. Furthermore, the desired flux observables would have to be built into the mode of

observation, thus limiting the range of accessible information unlike in the case of a fully exclusive experiment. At the present time when we are just starting to guess about the collective degrees of freedom, relevant to nucleus-nucleus collisions, a decision about the appropriate experiments seems premature. Let us wait to see what the next year of plastic ball and streamer chamber data analysis will tell us.

The fraction of unobserved particles in present 4π experiments is about 1/2, i.e. the neutrals. The plastic ball offers some promise as to neutron detection; however, with a different efficiency from that for charged particles. On the event-by-event basis, a 4π detection with about 15% efficiency for neutrons is of no real use unless the neutron multiplicity gets so high that even sampling them becomes significant, i.e. in Pb + Pb collisions. In such collisions, another indirect solution comes to mind; the fraction of clusters, d, t, ^3He , ^4He , will have such a high multiplicity that we might guess the neutron flux from the p:d and $^3\text{He}:t$ ratio in phase space, on the event-by-event basis. This might help to understand semiperipheral collisions, in the colder "spectator" regions of phase space. We shall come back to this aspect in the next chapter.

Finally, any nonuniformity of the detection efficiency can be a major obstacle in collective analysis. There is always a difficulty in the target plane, due to particle absorption, increased γ conversion, and multiple scattering. In addition, the streamer chamber cannot momentum analyze the 90° particles emitted along the magnetic field direction, and to some extent all particles moving along the camera viewing angles. The plastic ball appears, at first sight, to be free of such additional "blind spots". However, its finite energy range of particle identification, from

about 30 to 200 MeV/A, leads to trouble after transforming into the center of mass or any other moving frame; only about half the relevant phase space is covered. In the streamer chamber data analysis, we thus have to watch out for an instrument-induced flatness of the events, with a part of p_{\perp} missing. The plastic ball has a built in forward-backward anisotropy in the center of mass; its main strength thus lies with target fragmentation pattern analysis.

In general, all the three topics mentioned here, low multiplicities, lack of exclusivity, and detection efficiency anisotropy, result in a heavy leaning on Monte Carlo simulation of random but detector-typical background before significant information may be extracted.

III. Hybrid Analysis

In this chapter we shall sketch certain types of analysis in which there is a trigger particle selected, either by hardware or off line, and collective features of the event associated with it are considered at the same time. The simplest example is the familiar selection for small or large impact parameters²⁾, by requiring a high/low multiplicity of charged particles associated with a single reaction product. This is not an event-by-event analysis but just a selection of a restricted sample of events. Let us now look into examples that use a higher degree of exclusivity.

A. Localization of the impact plane

The concept for this experiment (yet to be carried out) originates from hydrodynamic model studies^{18,19)} of light projectile-heavy target reactions, like Ne + U. One approach towards testing the predictions of sideways collective flow, made by this model, is to identify $b = 0$ as closely as possible, by requiring cylinder symmetry about the beam axis and then look for directions of preferred emission of protons, clusters, etc. This selection is difficult because of the small cross section associated with $b \rightarrow 0$. To test hydrodynamics at finite impact parameters we have to select an effective b window and to localize the orientation of the impact plane, i.e. to find the plane that contains the beam axis and the two centers of the colliding nuclei.

This idea is illustrated in fig. 25 by the results of a hydrodynamical model calculation¹⁸⁾ of matter flux in Ne + U at 393 MeV/A, for various impact parameters. Invariant nucleon cross section contour levels are given, projected onto the impact plane defined by $\pm p_{\perp}$ and rapidity. The impact vector is always pointing to the positive p_{\perp}

direction, from the target to the projectile center. At $b = 0$ we observe total degradation of the incident projectile matter and momentum flux; the bulk of it is emitted at small rapidities and $50^\circ \lesssim \theta \lesssim 90^\circ$, with azimuthal (= cylinder) symmetry. At $b = 8$ fm, on the other hand, we find the target- and projectile-like regions of phase space preferentially populated. More accurately, the projectile remnant flux centers at a finite $\theta \approx 15^\circ$; it has acquired a finite total p_{\perp} , due to the collective "bounce-off" from the target surface. For $b = 6, 4, 2$ fm, the two flux families merge more closely but all the time exhibiting two peaks falling onto the impact plane. The "bounce-off" angle increases with b . Figure 26 shows a Ca + Pb event at 2.1 GeV/A that might correspond to $b \approx 6$ fm.

How would a collective analysis of exclusively measured events of Ne + U or Ca + Pb proceed in order to check this prediction? The nucleon and cluster multiplicity will be high enough, for all but the largest impact parameters, to perform a flatness analysis in terms of sphericity variables, obtaining $Q_1 < Q_2$ and the direction of Q_3 . Conveniently, the limiting case of cylinder symmetry, $Q_1 = Q_2$, $\alpha(Q_3) \rightarrow 0$, is contained in this. The directions of Q_2 and Q_3 define the impact plane. Of course, its orientation will only be approximately localized due to the finite particle number statistics of each event, perhaps to about $\pm 20^\circ$ in the azimuth. Alternatively, we might use the minimum spanning tree to identify the target/projectile particle families. The impact plane is then defined by the connecting main branch vector and the beam axis. After this, we shall rotate all the events into a common (arbitrary) impact plane orientation. Furthermore, we may sort the events into bins of Q_3 direction $\Delta\alpha_3$ in this plane, corresponding in the hydrodynamical model to bins of impact parameters (bounce-off angle).

Finally, we shall take an ensemble of about 500 to 1000 events per $0.1 \text{ GeV} < p_T < 0.2 \text{ GeV}$ bin, which means about 25 000 to 50 000 particle vectors per bin, at a mean multiplicity of about 50 in a minimum bias Ne + U experiment. Now we may construct invariant cross section contours and compare to the prediction of fig. 25 for the nucleon and cluster flux density distribution.

However, the check of hydrodynamics does not stop here. We may get one step further in looking at protons and clusters separately. This is significant because the regions of collective flux in phase space are relatively low in internal thermal energy, in the hydrodynamical model. In these regions, therefore, we expect an enhanced cluster abundance. Figures 27 and 28 illustrate this prediction for the proton and α -particle flux at $b = 6 \text{ fm}$. Chemical equilibrium conditions have been assumed for the final state of the hydrodynamical calculation¹⁸⁾, at densities below that of normal nuclear matter, resulting in a prediction of the flux carried by each nucleon or cluster species. It is obvious that the α -particle flux, fig. 28, exhibits the asymmetry and flatness of fluid dynamical flux predictions in a much more drastic way than the proton flux, fig. 27. The protons originate more specifically from the hot fireball zones (called head shock in the model terminology) and are emitted more spherically.

Such a comparison of data with theory will certainly be much more conclusive than anything we have done thus far. The corresponding phase space calculation, by means of the cascade model, will require a chemical equilibrium treatment of the final state of that model. Such calculations are also becoming available now²⁹⁾. The difference in the predictions of these two models should be that hydrodynamical collective flux leads to

a more narrow confinement of the spectator and participant particle families in phase space. The experimental effort, going into this test of reaction dynamics, is fairly high but still manageable.

A final remark is in order now about the term "hybrid analysis", that I use for such studies. They proceed from an event-by-event analysis (impact plane and bounce-off direction) to a single particle density distribution, as obtained from an ensemble of events binned according to their collective features.

B. Heavy spectator nuclear fragments and the bounce-off effect

A special case of the bounce-off mechanism in hydrodynamics arises if, in a reaction like Ca + Pb, a large fraction of the target spectator remains intact, with the emission of a heavy fragment that carries most of the target part of the collective momentum flux. This type of event will be associated with rather large impact parameters. In hydrodynamics terminology, the mechanism would be understood in terms of a collective pressure field associated with the high density in the target-projectile overlap region that is localized on the surface of the heavy target nucleus. The target spectator region is pushed to the side, as is the projectile remnant. The energy transfer is relatively small (unlike in central collisions) and shared equally between the target and projectile remnants. It will be sufficient to fragment the small projectile remnant into nucleons and light clusters, but in the target remnant there may be regions left cold enough in order to survive as heavy fragments, still carrying the collective bounce-off momentum transfer. From elastic α -particle scattering at 180° it is known that the target mean field can impart several GeV/c of recoil momentum without fragmentation.

The resulting final state: light projectile fragments, near beam velocity, are emitted at small but finite $\theta \lesssim 10^\circ$. Also on the projectile side in the impact plane, we shall observe the expansion products from the hot overlap zone, mostly nucleons at about midrapidity. The heavy target remnant recoils to the opposite direction in the impact plane. The experimental program is then to

1. Identify the projectile fragment family and determine the corresponding thrust direction that, together with the beam direction, fixes the impact plane and the projectile bounce-off angle.
2. Identify the "fireball" particles near midrapidity. Their number is a measure of the size of the overlap zone and, thus, of the impact parameter. Their total energy approximates the energy transfer between target and projectile (the degree of inelasticity).
3. Identify the target fragments, triggering the experiment by the occurrence of a heavy ($A \gtrsim 50$) nucleus that is slow in the laboratory frame. At 10 MeV/A, such a fragment carries $\gtrsim 7$ GeV/c of collective momentum! At 2 GeV/A incident ^{40}Ar energy, about 30 projectile fragment nucleons balancing this momentum would be distributed around $\theta \approx 5^\circ$.

In connection with this type of expected event, the remark has often been made that all its features follow directly from energy/momentum conservation. This is not true, however. Of course, any final state is consistent with the conservation laws, but the hydrodynamical model predicts a much sharper focusing of the momentum flux into the two bounce-off directions than any phase space model (cascade), due to the collective pressure gradient established in the interaction zone. The shape of the colliding nuclear matter distribution, at given impact

parameter, plays a decisive role in the orientation of the resulting pressure field, unlike in cascade calculations in which each binary nucleon scattering is assumed to proceed as in free space, and the shapes are of secondary importance, affecting the outcome only through subsequent rescattering. A different way of stating this: the overlap zone in such a semiperipheral event has a thickness of only about two mean free paths, in the cascade view of things. These two binary scatterings per nucleon are governed by free N-N collision phase space, with little chance of a cooperative effect setting in that could simulate the collective deflection of flow in hydrodynamics. Thus, an event with sharp focusing of the flux is rare in the cascade model, whereas it is predominant in the hydrodynamical model. Of course, the applicability of hydrodynamics appears to come to its very limit in this situation. Zero mean free path is assumed locally, in the rather small subvolume of target and projectile overlap, which accommodates only about two binary collisions, in the cascade approach.

This rather risky theoretical situation has attracted several experiments, reported at this conference^{21,22}). Figure 29 shows a sketch of one²¹), using three major components: a set of detectors for heavy, slow target fragments inside a vacuum chamber; a multiplicity array for fast particles surrounding the forward hemisphere of the chamber (fireball products); and the segmented plastic wall array, identifying the projectile fragment flux distribution at small forward angles by means of time of flight and specific ionization measurement. The data of this experiment, which is only exclusive to the extent required by the sought observables, are not yet fully analyzed. We are also waiting for a cascade model treatment of the bounce-off effect.

C. Pion condensation search

Let us now reach out, with some speculative remarks, beyond the familiar territory of models. Of course, hydrodynamics will only be conclusively tested in exclusive analysis, and in this way we may indirectly approach the still evasive conditions at high density in the transient, short-lived state before expansion. One qualitative step further into the unknown do we go in thinking about phase transitions and their possible characteristic observables, because such theories require a detailed microscopic state of nuclear matter, for the short transient time scale of some 10^{-23} s, beyond the development towards local equilibrium or the onset of collective flux. At Bevalac energies, pion condensation is the only likely candidate for a phase transition because the total energy density of at most 0.8 GeV per cubic Fermi, reached at density $\rho = 4\rho_0$ in a 2 GeV/A Ca + Ca collision, falls well below the present estimates for a quark matter transition²³⁾.

Let us disregard, for the moment, the critical questions about short lifetime, finite size, and high temperature of the fireball, assuming that a small but finite fraction of near-central collision events result in pion condensation. This results in symmetry breaking²⁴⁾; a spin-isospin ordered lattice is being established in the interaction zone, leading to long-range orientation along a plane that is fluctuating from one event to the other. This state may be reflected in an emission anisotropy because the nucleons in the remote regions of target and projectile, streaming into the overlap zone where a condensate is already established, will scatter anisotropically with respect to the lattice direction (critical opalescence). Thus, at least at $b \approx 0$, there are no leading fragments but the event still shows no cylinder symmetry. We are referring to a collision of equal size nuclei.

The experiment should thus select nonspherical events of maximum multiplicity, no leading particles, and a thrust of sphericity orientation towards large η . Unfortunately, such an event pattern might also be caused by hydrodynamical flow, at small but finite impact parameters (fig. 19). We would then localize nothing but the impact plane. We need another additional observable to be selective to pion condensation. Can we make use of the spin orientation along the lattice? One idea might be to identify a signal of magnetic moment orientation in observing γ -emission anisotropy. However, let us stay within the capabilities of existing instrumentation, like the streamer chamber. We may think, then, about a polarization measurement of the produced particles. Proton polarization can be measured by secondary scattering from spin zero nuclei. This would require something like a carbon foil surrounding the target, measuring the up/down asymmetry of secondary interactions in it. Each event provides a sufficient number of emitted protons, such that at least one such reaction takes place, per event, even in a thin foil. However, the analyzing power of double scattering is low, and we may be unable to satisfy statistical requirements, within the limits imposed by the effort of exclusive event analysis.

An alternative approach may be to look at Λ particle polarization¹⁰). The Λ particles produced in the interaction decay in flight, away from the primary vertex, $\Lambda \rightarrow \pi^- + p$ with 67% branching ratio. In this weak decay, the Λ polarization direction is preserved (by parity nonconservation) in the spatial orientation of the Λ -p production plane. The analyzing power of this process is high (0.64). The rationale would be that Λ particles are produced in the high energy density zone, i.e. in the pion condensate. They rescatter from the lattice, orienting

their spin direction relative to it. We would thus have to obtain an ensemble of high multiplicity, no leading particle, nonspherical events with a Λ in it. This set of requirements implies a lot of running time because the mean Λ multiplicity in Ca + Ca central collisions at 2.1 GeV/A is only about 0.08. We should gather several thousand Λ -producing events, to look for a change of polarization with the orientation of Λ emission relative to the event asymmetry plane, as resulting from sphericity analysis of the event protons. Unless a 4π - Λ trigger is used--a detector system by far exceeding familiar experiment dimensions at the Bevalac--this amounts to gathering about 200 000 central trigger events in the streamer chamber (≈ 200 Bevalac hours), scanning all of them for Λ events, and exclusively analyzing the resulting sample of several thousand. Figure 30 shows how Λ particles are identified from an invariant mass analysis of the measured negative and positive track rigidity in a "Vee" event¹⁰⁾. Competing Vee-producing events are $K^0 \rightarrow \pi^+ + \pi^-$ decay and $\gamma \rightarrow e^+ + e^-$ conversion; they are discriminated by invariant mass analysis.

We see that the effort is very high; we are certainly approaching the level of particle physics experiments here. Furthermore, this experiment proposal is based on theoretical dreams. In particular, one might argue that the Bevalac maximum energies, at which we reach the Λ production threshold, come along with reaction temperatures that are beyond the critical temperature for pion condensation. With considerations such as these, we have obviously exhausted our present experimental and theoretical capacities. They may still serve for an orientation as to what lies ahead.

IV. Conclusions

In this talk, I have focused entirely on multiparticle correlations because this field is new and relatively unfamiliar to all of us, but our experimental developments, like the plastic ball or the streamer chamber, do already allow for this type of analysis. Two particle correlation analysis is certainly as promising a tool, to proceed beyond single particle inclusive observables. Such correlations as

- a. "Anomalous" decay studies by $\alpha \rightarrow d + d$ invariant mass reconstruction with the HISS spectrometer²⁵⁾,
- b. Di-lepton measurements²⁶⁾,
- c. Back-to-back proton or pion emission correlation²⁷⁾,
- d. Proton-proton quasifree scattering kinematical correlation²⁸⁾,
- e. Identical pion and nucleon correlation²⁹⁾ at $\Delta\vec{p} \rightarrow 0$ (Hanbury-Brown, Twiss effect), and
- f. "Vee" events from Λ , K^0 decay, and γ conversion, imbedded in the final state¹⁰⁾

are being actively pursued at the present time, and contributions to this conference illustrate their richness in information.

Let me end with some conclusions about exclusive, event-by-event analysis:

A. As examples of collective analysis of the final state, we have described the concepts of thrust, sphericity, and the minimum spanning tree. The first two lead to the construction of multi-axial 3-dimensional surfaces, representing the density distribution of momentum and square momentum flux, respectively. Two jet structure, flatness, leading particle motion, and the orientation of the impact plane, as well as zero impact parameter selection by cylinder symmetry, are the observables most

easily accessible in this framework. The minimum spanning tree is the most flexible approach, applicable to any 2- or 3-dimensional, \vec{r} or \vec{p} or E space representation of the event. It identifies any clustering or particle family structure, depending on the choice of metric, and thus appears to be suitable for exposing unexpected features for which we do not yet have theoretical prejudices.

Furthermore, we should exploit scalar quantity correlations in the events, such as proton, pion, cluster multiplicities, or $|p_{\perp}|$ and $|p_{\parallel}|$ sums and the total transverse energies carried by various particle species.

B. To apply collective analysis, we need a sufficient number of microscopic degrees of freedom per collective degree of freedom. Monte Carlo simulation of events becomes extremely significant, to assess the essaying power of collective analysis. Thus, we should be delighted, rather than frightened, about the high multiplicities of particles in Bevalac energy collisions! Proton (and neutron) multiplicities are always adequate, but pion and cluster statistics will be marginal. At CERN PS energies of up to 15 GeV/A, pion analysis will come to the foreground, and strange particle statistics will be marginal.

Looking ahead to Bevalac Pb + Pb reactions at 1 GeV/A, with proton multiplicities exceeding 100, or to VENUS or CERN ISR reactions producing even more pions, we shall reach a point at which individual particle momentum reconstruction becomes both overwhelmingly tedious and perhaps unnecessary. Calorimetric experiments that measure local averages of particle, energy, or charge flux appear more appropriate. However, we shall then lose some of the nice aspects of fully exclusive identification, for example the possibility to construct any desirable two particle correlation observable. Furthermore, at Bevalac energies, a

large fraction of the final state particles will be too low in energy to apply familiar calorimetry. New experimental designs, not provided by present particle physics, have to be developed.

C. The presently available $4\pi^-$ instrumentation, i.e. the plastic ball and wall, the streamer chamber, and emulsions, are perfectly suitable for us to test conclusively the dynamical models, discussed now. Kinematical equilibrium vs transparency, local chemical equilibrium, etc. are approached in observables like event-by-event p_{\parallel} to p_{\perp} ratios, cluster and nucleon flux comparison, and the distribution of the charge to neutral ratio in phase space. For example, in collisions of zero isospin nuclei like ^{40}Ca with high isospin targets, the distribution of the $t:^3\text{He}$ ratio in phase space, along with a determination of the impact plane, will serve to pin down the flux pattern of projectile and target matter and the extent of equilibration (mixing).

Beyond this, the selection of events corresponding to finite impact parameter domains, by cylinder symmetry for $b \rightarrow 0$ and impact plane plus "bounce-off" pattern identification for finite b , will enable us to discriminate phase space/cascade mechanisms from collective fluid dynamics patterns. The overall result of this might be that one of the models will be substantiated, in all its predicted observable features, by the features of a certain class of reaction, like $\text{Fe} + \text{Fe}$ or $\text{Ca} + \text{Pb}$, to such a degree that its implications about density and temperature in the transient compressional phase gain credibility. Such that, although we are still not finding direct probes for the ratio of potential (compressional) to thermal energy, as a function of reaction time, the features of the nuclear matter equation of state become known.

D. Beyond our present model discussion of hydrodynamical collectivity versus phase space/cascade statistics, the guidance provided by theory is scarce, as far as suitable observables, corresponding to phase transitions, are concerned. If pion condensation occurs, and if it leads to a macroscopic plane of lattice order in the collision (and not to a multitude of randomly ordered domains as in a ferromagnet), we may identify it by decay anisotropy, detected event by event, and by additional probes of the spin/magnetic moment orientation.

Finally, beyond the guidelines and prejudices established by theory, there is always the empirical approach. Let us look, by means of exclusive analysis, for unexpected and surprising features of the event.

This work was supported by the Director, Office of Energy Research, Division of Nuclear Physics of the Office of High Energy and Nuclear Physics of the U.S. Department of Energy under Contract W-7405-ENG-48 .

References

1. See the review talk of S. Nagamiya at this conference.
2. R. Stock, et al., *Phys. Rev. Lett.* 44 (1980) 1243;
S. Nagamiya, et al., LBL preprint 12123, 1981.
3. S.Y. Fung, et al., *Phys. Rev. Lett.* 40 (1978) 292;
A. Sandoval, et al., *Phys. Rev. Lett.* 45 (1980) 874.
4. V.D. Aksinenko, et al., *Nucl. Phys.* A348 (1980) 518.
5. M.R. Maier, H.G. Ritter, and H.H. Gutbrod, *IEEE Trans. on Nucl. Sci.* 27 (1980) 42.
6. H.G. Baumgardt, E.M. Friedlander and E. Schopper, contribution to this conference;
K.B. Balla, contribution to this conference.
7. See the talk of W.J. Willis at this conference.
8. H. Stöcker, et al., *Z. Phys.* A243 (1979) 173.
9. A. Mekjian, *Phys. Rev.* C17 (1978) 1051.
10. J. Harris, et al., LBL preprint 12334, 1981, to be published in *Phys. Rev. Lett.*
11. GSI-LBL streamer chamber collaboration, unpublished data.
12. J. Cugnon, T. Mitzutani, and F. Vandermeulen, Caltech preprint MAP-10, 198C;
C. Riedel and Y. Yariv, private communication;
J. Cugnon, *Phys. Rev.* C22 (1980) 1885.
13. R. Hanbury-Brown and R.Q. Twiss, *Nature* 178 (1956) 1046;
G. Goldhaber, S. Goldhaber, W. Lee and A. Pais, *Phys. Rev.* 120 (1960) 300.
14. S.L. Wu and G. Zobernig, *Z. Phys.* C2 (1979) 107.
15. S. Brandt and H. Dahmen, *Z. Phys.* C1 (1979) 61.
16. J. Dorfan, SLAC reprint PUB 2623, 1981.

17. J. Knoll, talk at this conference.
18. H. Stöcker, J.A. Maruhn and W. Greiner, Phys. Rev. Lett. 44 (1980) 725;
H. Stöcker, et al., LBL preprint 11774, 1981;
H. Stöcker and L.P. Csernai, private communication.
19. J. Kapusta and D. Strottman, Phys. Rev. C23 (1981) 1282, and Los Alamos preprint LA-UR-81-795, 1981;
A.A. Amsden, F.H. Harlow and J.P. Nix, Phys. Rev. C15 (1977) 2059.
20. J.D. Stevenson, Phys. Rev. Lett 45 (1980) 1773.
21. A.I. Warwick, et al., contribution to this conference;
W.G. Meyer, H.H. Gutbrod, Ch. Lukner and A. Sandoval, Phys. Rev. C22 (1980) 179.
22. U. Lynen, talk at this conference.
23. E.V. Shuryak, Physics Reports 61 (1980) 72;
J. Rafelski, contribution to this conference.
24. N.K. Glendenning, talk at this conference;
M. Gyulassy, Proc. Hakone SKeminar 1980, K. Nakai, editor;
N.K. Glendenning and A. Lumbroso, LBL preprint 12108, 1981.
25. D. Greiner, et al., Bevalac experiment proposal;
E.M. Friedlander, et al., Phys. Rev. Lett. 45 (1980) 1094.
26. D. Antreasyan, et al., CERN-EP/80-75, 1980.
27. J.W. Harris, et al., BAPS 25 (1980) 560.
28. I. Tanihata, et al., contribution to this conference.
29. S.Y. Fung, et al., Phys. Rev. Lett. 41 (1978) 1592;
C.C. Lu, et al., Phys. Rev. Lett. 46 (1981) 898;
W.A. Zajc, et al., contribution to this conference;
F. Zarbakhsh, et al., contribution to this conference;
G.I. Kopylov and M.J. Podgoretsky, Sov. J. Nucl. Phys. 18 (1974) 336.

Figure Captions

- Fig. 1. Streamer chamber view of a central $^{40}\text{Ar} + \text{KCl}$ interaction at 1.3 GeV/A.
- Fig. 2. The same event as fig. 1, after measurement.
- Fig. 3. Correlation between negative pion and total charged particle multiplicity in Ar + KCl at 1.3 GeV/A. The smooth lines give contours of event frequency. Events that produce a Δ particle are given as crosses.
- Fig. 4. Preliminary data from an exclusive analysis of Ar + KCl central collisions at 1.8 GeV/A for the event-by-event values of total $\frac{2}{\pi} |p_{\perp}|$ and $|p_{\parallel}|$ in the center of mass, as normalized by the multiplicity M of charged particles. The lower part shows Ar + Pb at 0.8 GeV/A with p_{\parallel} referring to the fireball center of mass.
- Fig. 5. The laboratory momentum vectors of the event shown in figs. 1 and 2 in a side view. The beam is in x direction.
- Fig. 6. Top view of the same event, as transformed into the center of mass system.
- Fig. 7. Side view of the same event in the c.m. system. Four jets are clearly distinguished in this projection.
- Fig. 8. The same event, as viewed in beam direction.
- Fig. 9. Central collision of $^{40}\text{Ca} + ^{40}\text{Ca}$ at 2.1 GeV/A, exhibiting the typical forward focus in the lab frame of equal mass central collisions.
- Fig. 10. Central collision of $^{40}\text{Ca} + \text{Pb}$ at 2.1 GeV/A. Note the different emission pattern in the target fragmentation region.
- Fig. 11. Another example of $^{40}\text{Ca} + \text{Pb}$ at 2.1 GeV/A, showing complete projectile energy degradation.

Fig. 12. Contour plot of invariant $\text{Ar} + \text{KCl} + \bar{\pi}^-$ cross section, for central collisions at 1.8 GeV/A. The dashed lines correspond to an isotropical pion source at midrapidity.

Fig. 13. Distribution of polar angle in the c.m. system of $\bar{\pi}^-$ produced in $\text{Ar} + \text{KCl}$ at 1.8 GeV/A.

Fig. 14. Distribution of polar angle in the c.m. system of the $\bar{\pi}_3^-$ sphericity direction, from an event-by-event analysis of $\text{Ar} + \text{KCl} + n\bar{\pi}^-$, $n \geq 4$.

Fig. 15. Event frequency contour lines, in the plane of sphericity vs flatness/coplanarity, from collective analysis of the negative pions in the c.m. system of $\text{Ar} + \text{KCl}$ at 1.8 GeV/A.

Fig. 16. Projection of fig. 15 onto the sphericity axis.

Fig. 17. Same plot as fig. 16, now showing the ratio of data events to Monte Carlo events, for each bin in S_1 . The ratio is compatible with one, for all S_1 .

Fig. 18. Plot of event frequency contours, in the plane of maximum elongation $(1 - S_2)$ vs polar orientation of $(1 - S_2)$, resulting from sphericity analysis of the participant protons in a cascade model calculation of $^{36}\text{Ar} + ^{36}\text{Ar}$ at 360 and 1120 MeV/A. Multiplicity cuts corresponding to a minimum bias trigger ($m \geq 1$) and to a central collision selection are shown.

Fig. 19. Configuration space plot of the density development with time, from a hydrodynamic calculation of equal mass nuclei colliding at three different impact parameters.

Fig. 20. Results of nucleon thrust analysis of the hydrodynamical calculation, shown in fig. 19, exhibiting T as a function of b/b_{max} and bounce-off angle relative to the beam axis.

- Fig. 21. Sketch of the global features of a central $A + A$ collision, as predicted by hydrodynamical and cascade models.
- Fig. 22. Plot of polar vs azimuthal angle in the c.m. system of charged particles in a central Ar + KCl event at 1.8 GeV/A.
- Fig. 23. Sketch of an application of the minimum spanning tree analysis to three groups of particles, clustering in a 2-dimensional representation.
- Fig. 24. Sketch of the plastic ball, plastic wall 4--detector system.
- Fig. 25. Hydrodynamical model: contours of invariant nucleon + cluster cross section, projected onto the impact parameter plane, for $b = 1, 2, 4, 6, 8$ fm, in Ne + U collisions at 393 MeV/A.
- Fig. 26. Streamer chamber view of an event $^{40}\text{Ca} + \text{Pb}$ at 2.1 GeV/A, which exhibits the qualitative features of a bounce-off reaction.
- Fig. 27. Hydrodynamical model: contour plot for impact parameter $b = 5$ fm in Ne + U, showing the part of matter flux emerging in free protons.
- Fig. 28. The same plot, for π -particle emission, in chemical equilibrium.
- Fig. 29. Sketch of an experiment designed to identify the bounce-off effect predicted by the hydrodynamical model. The three main components are shown: a set of detectors for slow, heavy target fragments inside a vacuum chamber; surrounding it is a multiplicity array for fast fireball fragments; farther downstream, the segmented plastic wall registers projectile remnants at $\theta < 9^\circ$.
- Fig. 30. Invariant mass plot constructed from "Vee" events in Ar + KCl central collisions at 1.8 GeV/A. The branches due to $\Lambda \rightarrow p, \bar{\Lambda}$ and $K^0 \rightarrow \pi^+ \pi^-$ are exhibited.

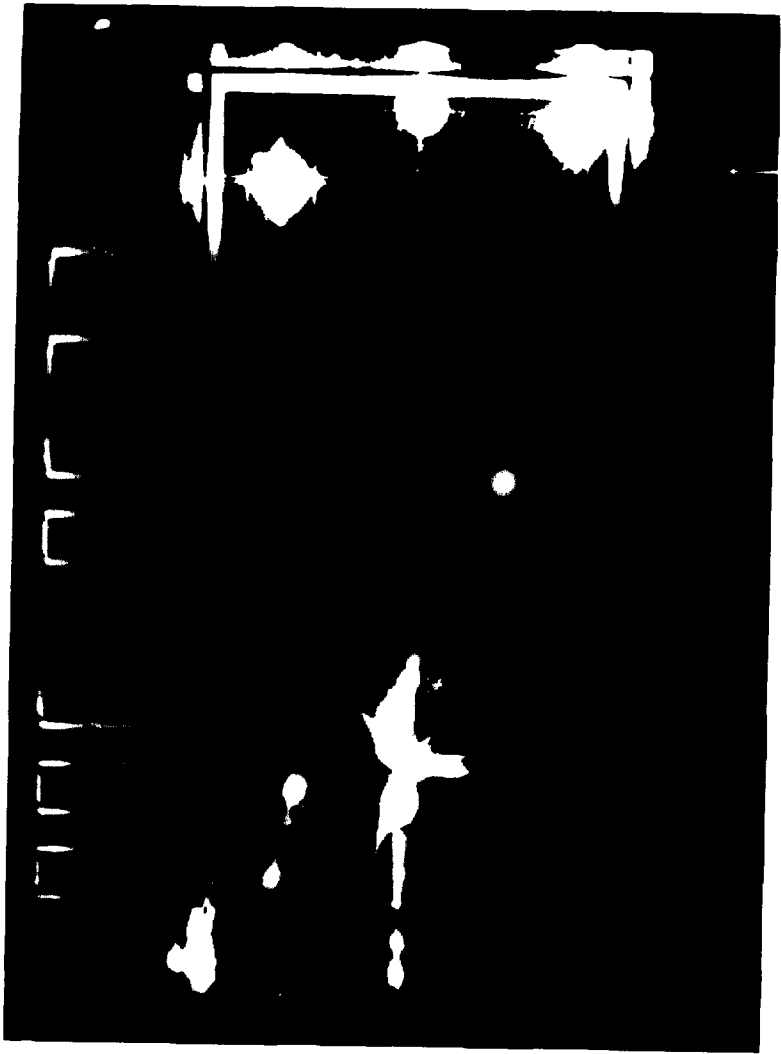
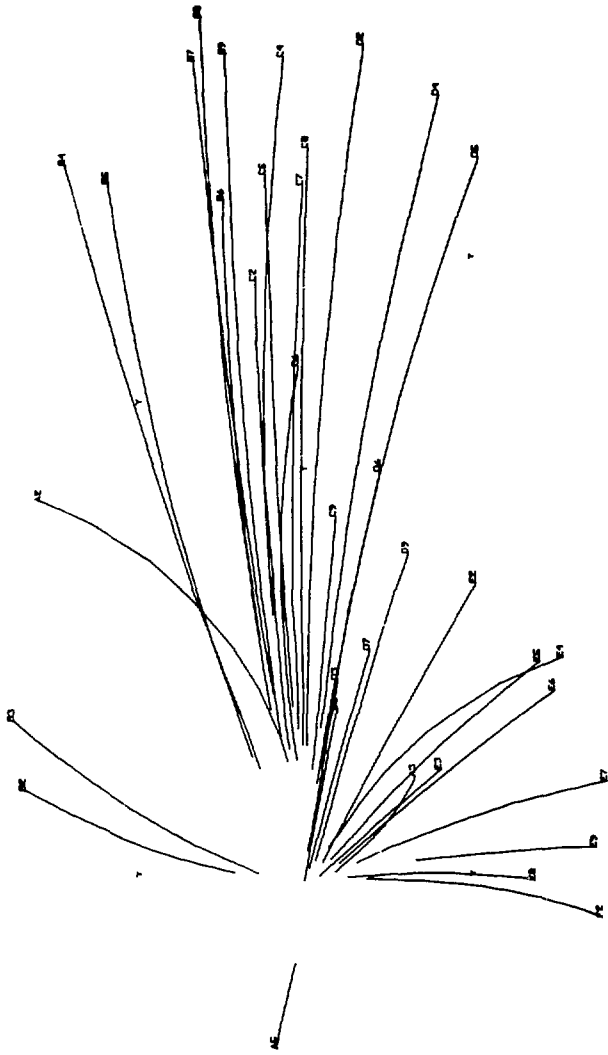


Fig. 1



6052702.

XBL 816-10164

Fig. 2

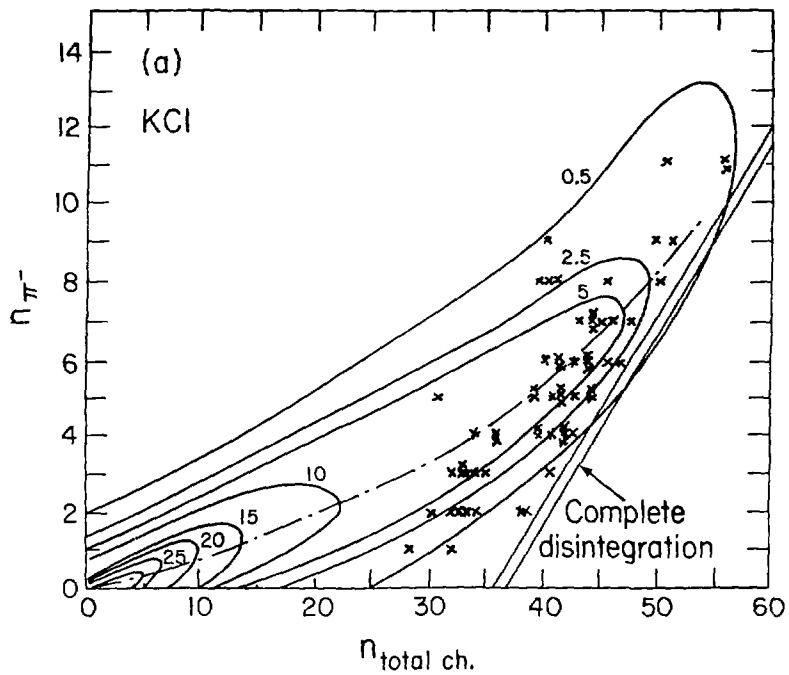


Fig. 3

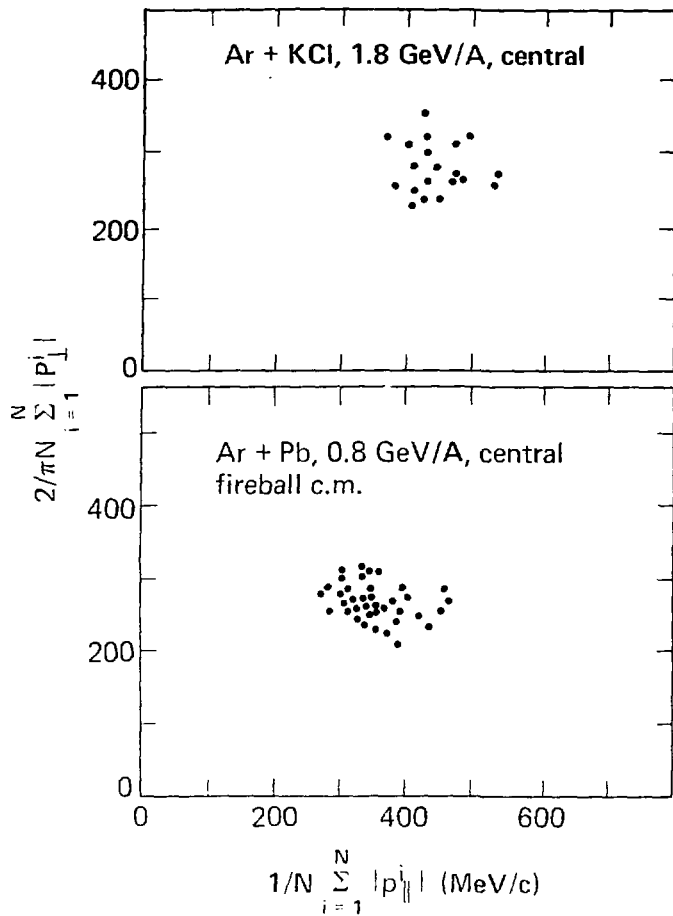


Fig. 4

PHYS. REV. D 120 1

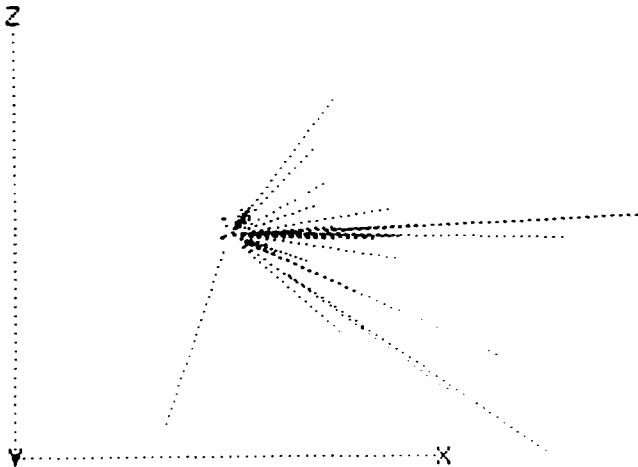


Fig. 5

XBL 816-5045

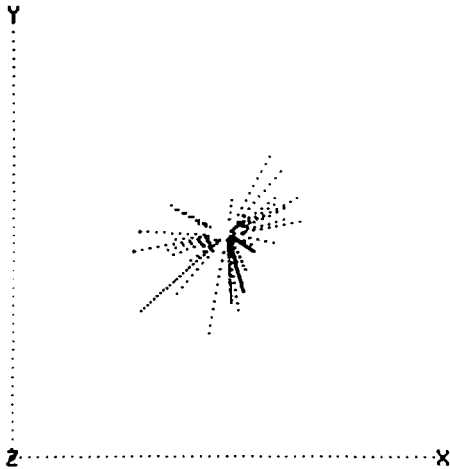


Fig. 6

XBL 816-5047

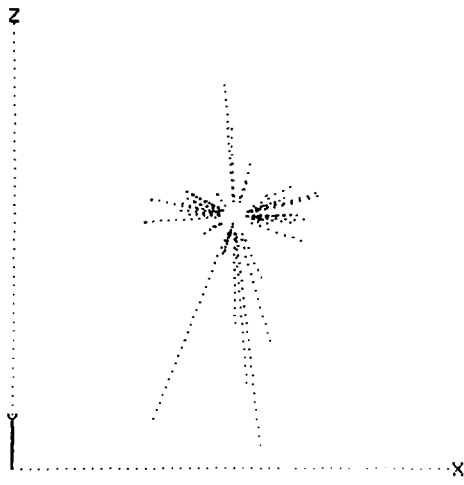


Fig. 7

XBL 816-5044

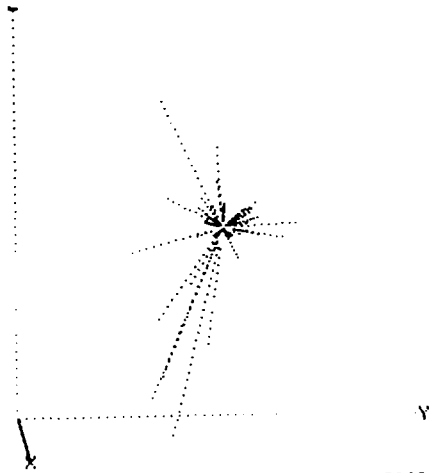


Fig. 8

XBL 816-5048



Fig. 9



Fig. 10



Fig. 11

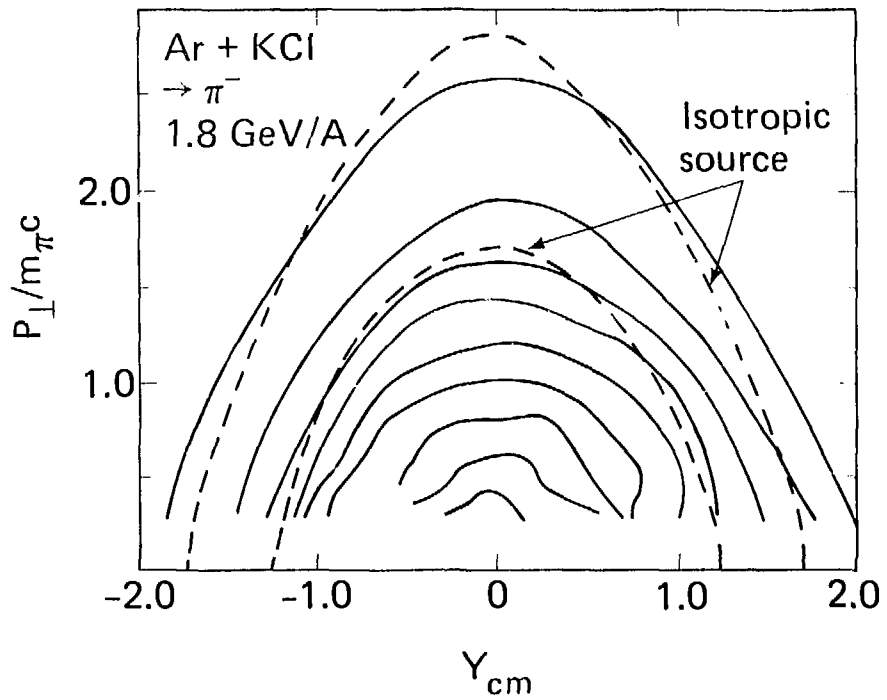


Fig. 12

XBL 818 1257

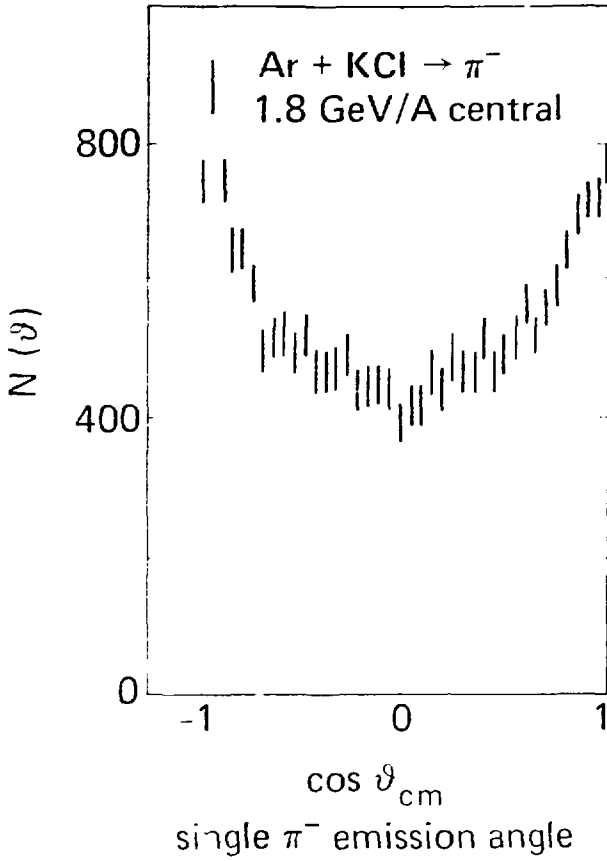


Fig. 13

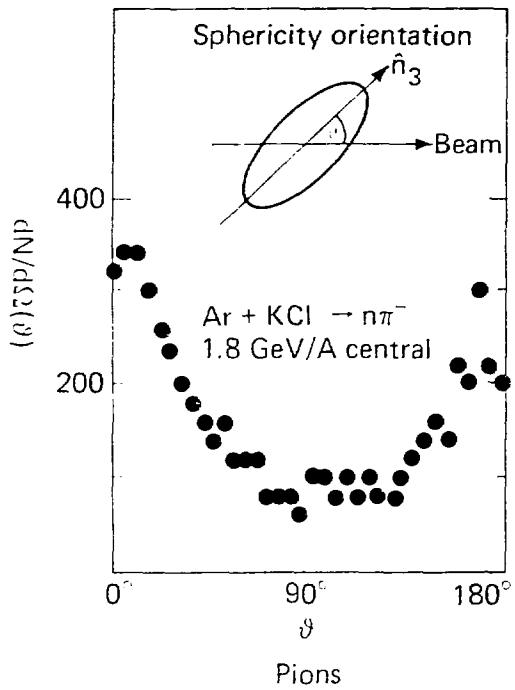


Fig. 14

XBL 818 1261

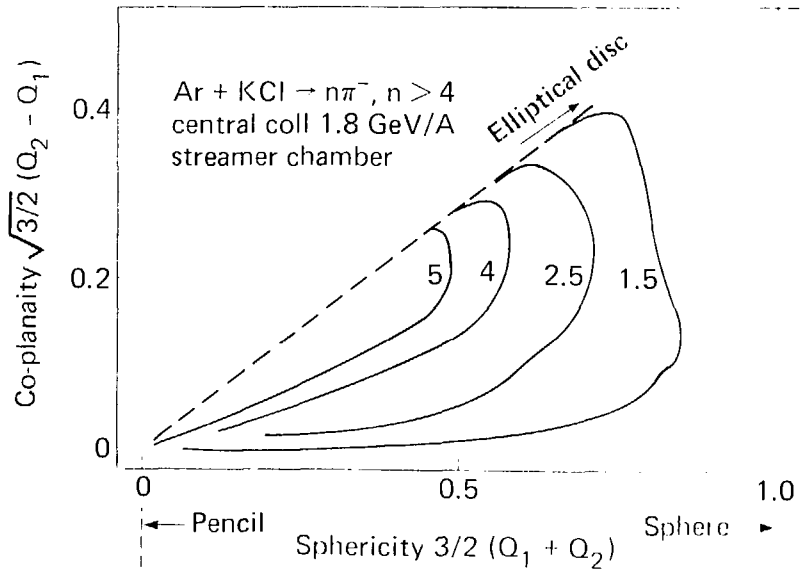


Fig. 15

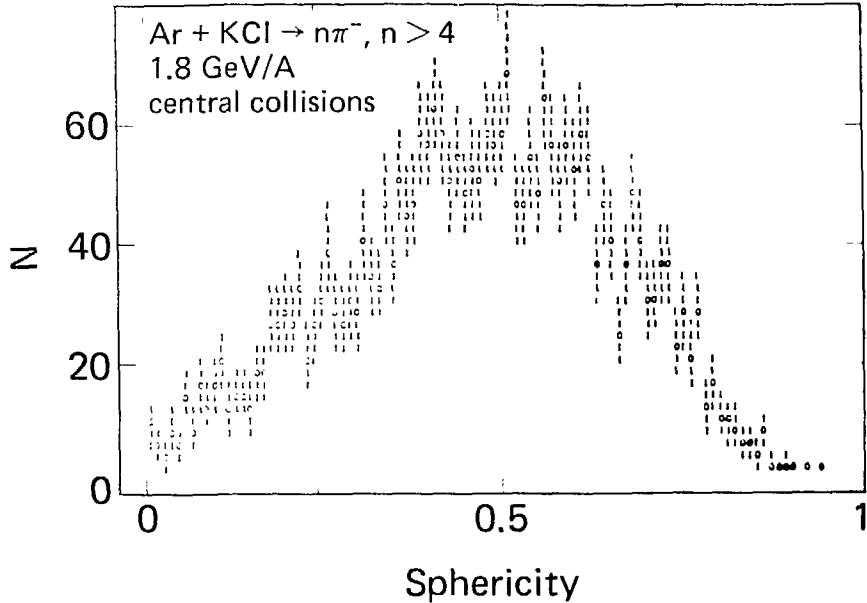
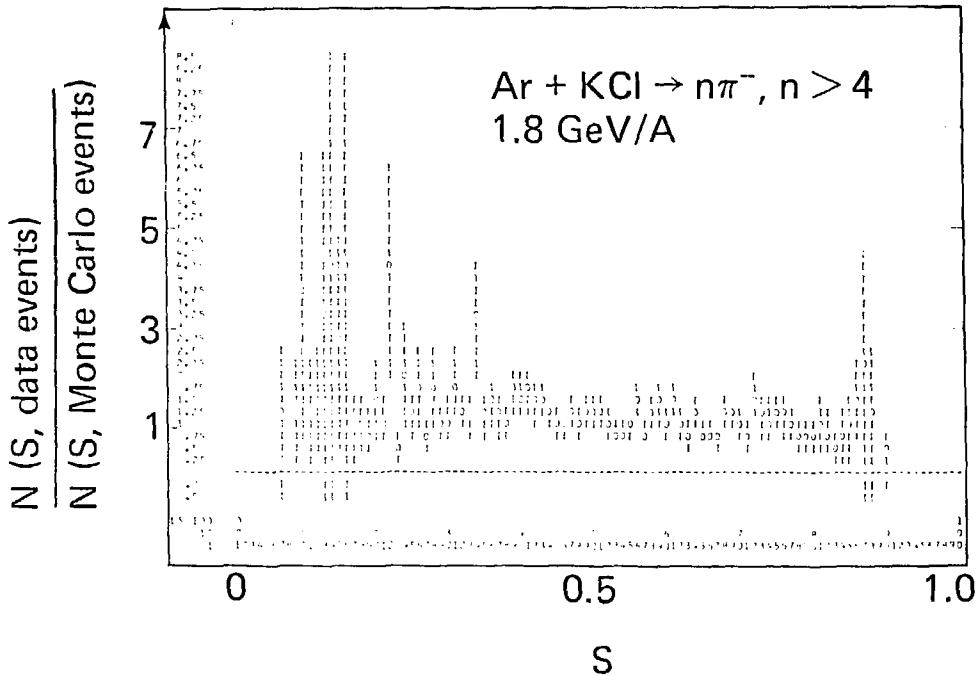


Fig. 16

XBL 818 1258



→ At $\langle n\pi^- \rangle \approx 8$, the sphericity signal does not stand out above Monte Carlo random sampling event sphericities!

Fig. 17

Ar + Ar → protons, Cascade model
Knoll, Riedel, Yariv

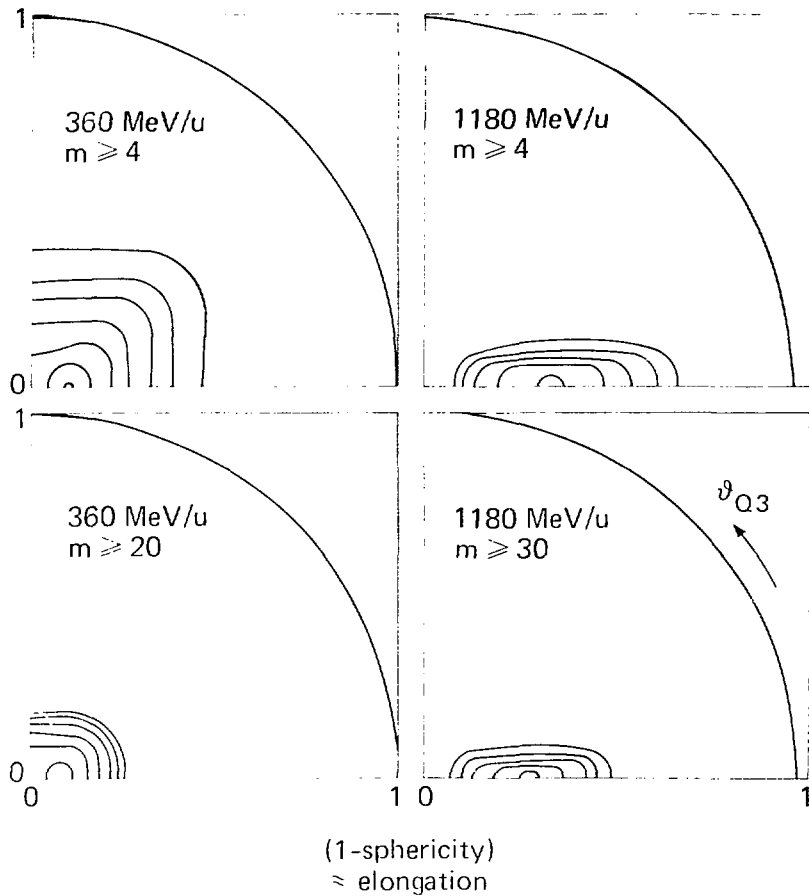


Fig. 18

NRL 818 1265

A + A

182 MeV/A

CM

$b = 0.8 b_{max}$

$b = 0.4 b_{max}$

$b = 0$

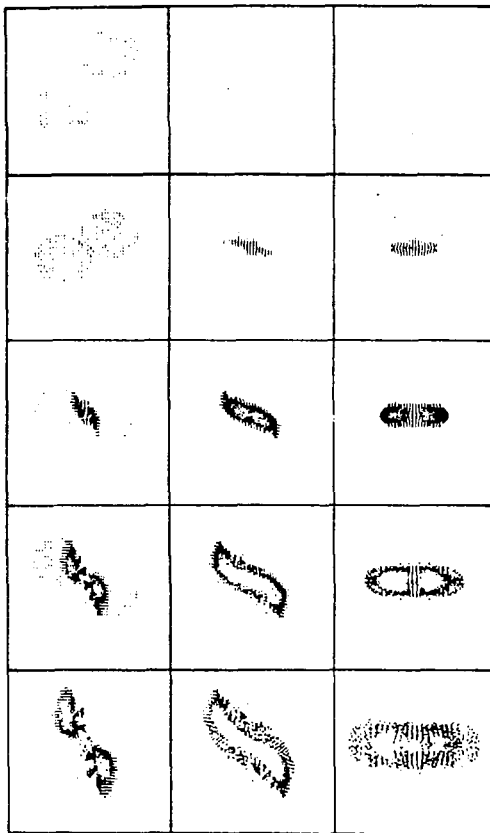


Fig. 19

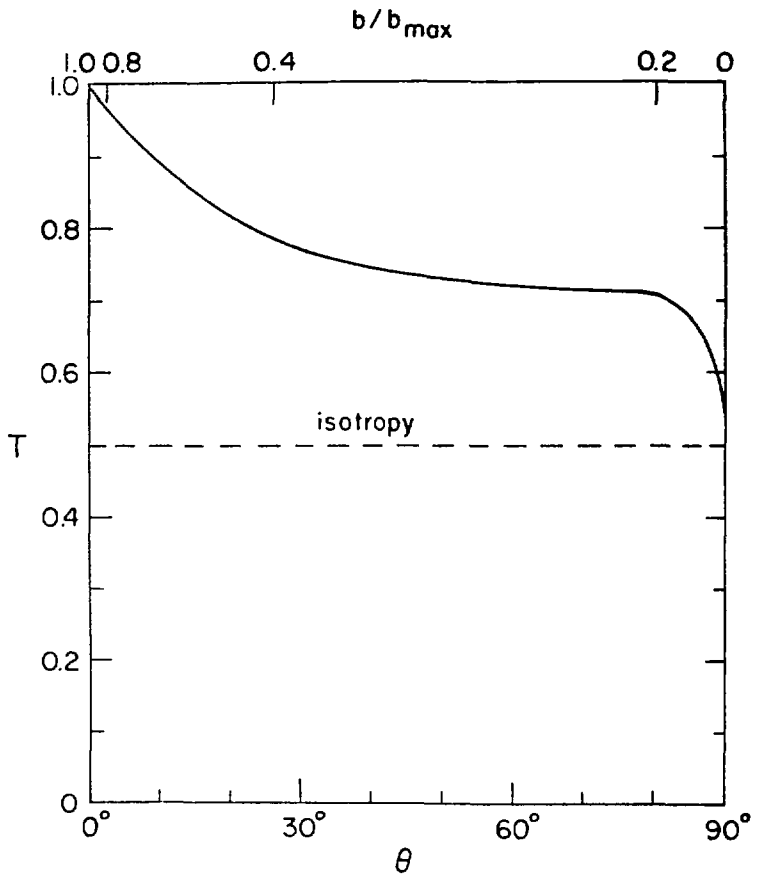


Fig. 20

Symmetric collisions in CM

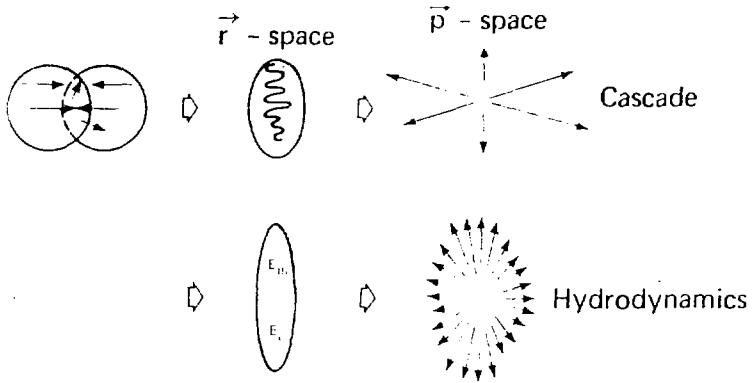


Fig. 21

ABR 816 1,200

Cascade: Not scale and E invariant

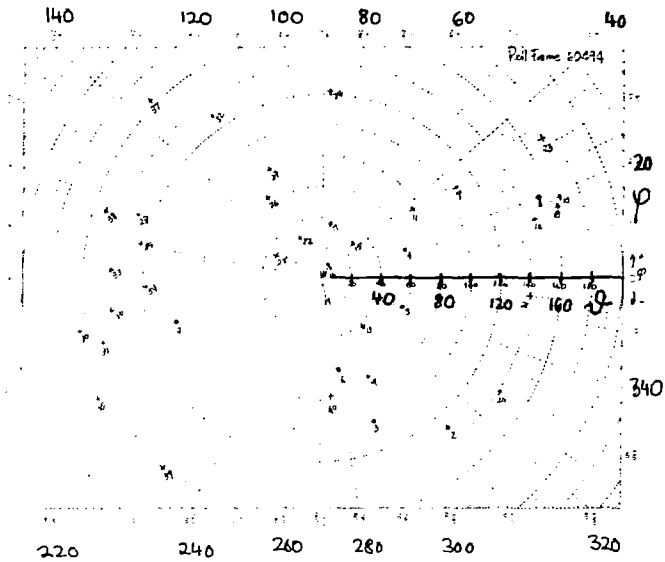
→ sphericity increases with A
decreases with E
thrust in beam direction

Hydrodynamics: A invariant

sphericity increases with E?
thrust \perp to beam

Nature ?

Ar + KCl \rightarrow charged particles , 1.8 GeV/A



θ polar, φ azimuthal c.m. system angle

Fig. 22

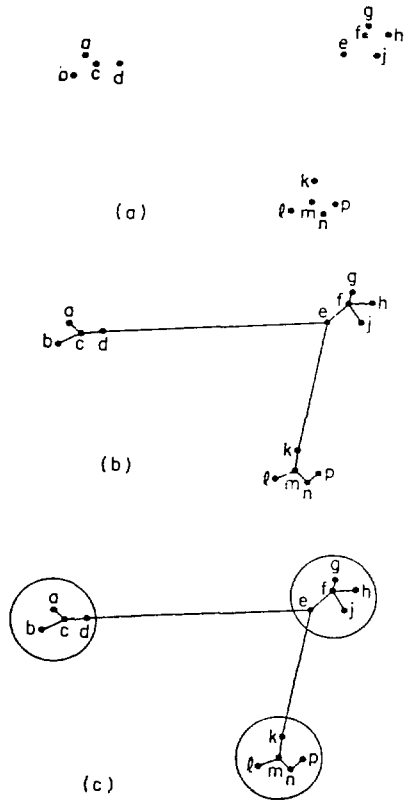
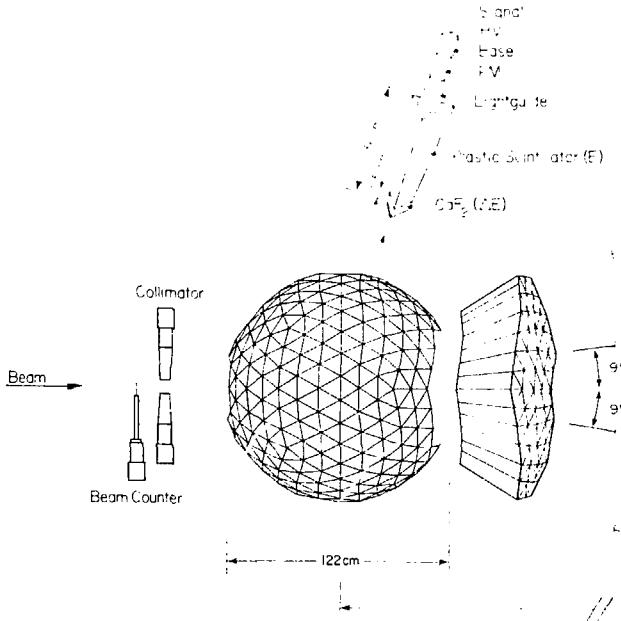


Fig. 23

PLASTIC BALL

655 modules + 160



PLASTIC WALL

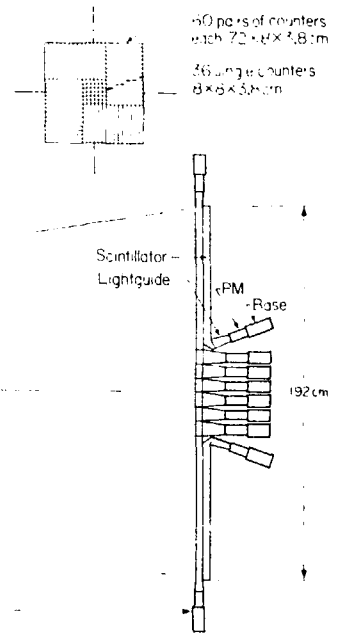


Fig. 24

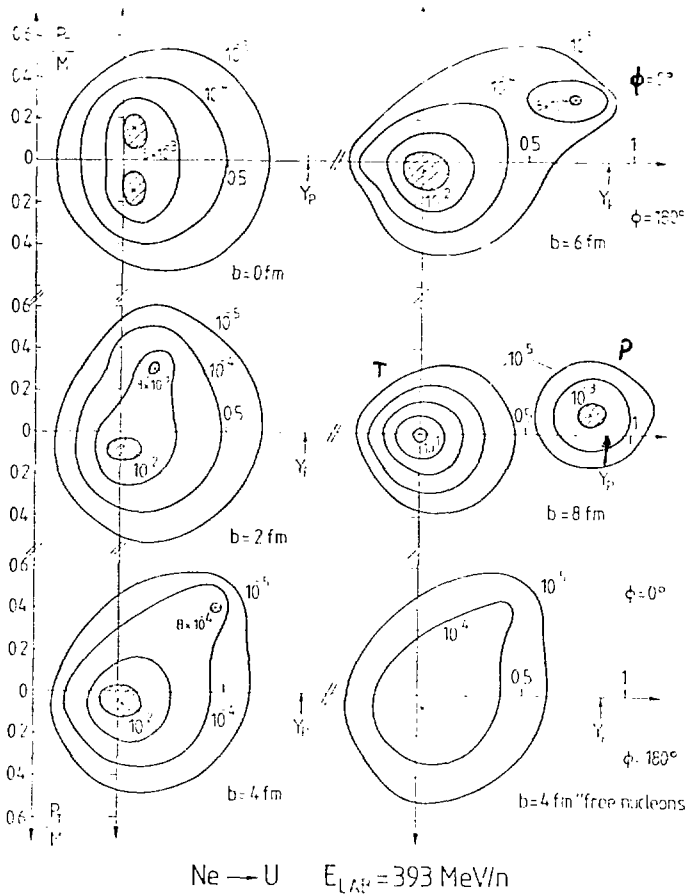


Fig. 25



Fig. 26

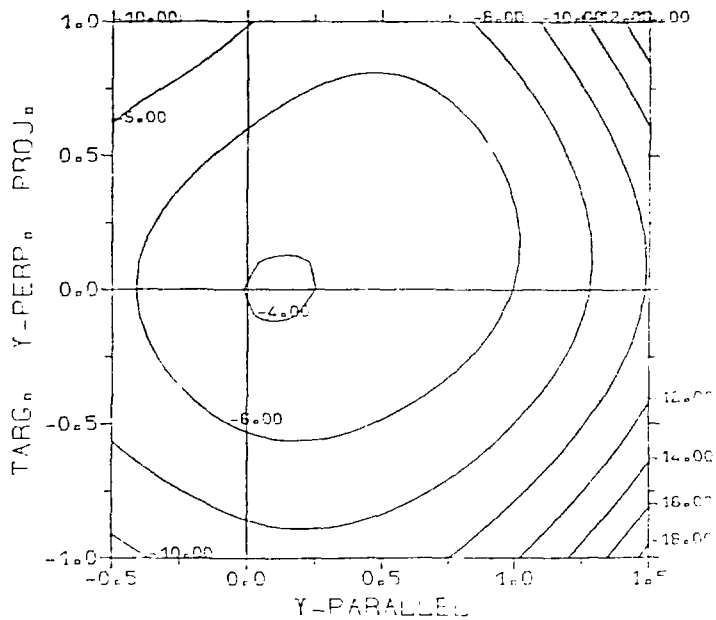
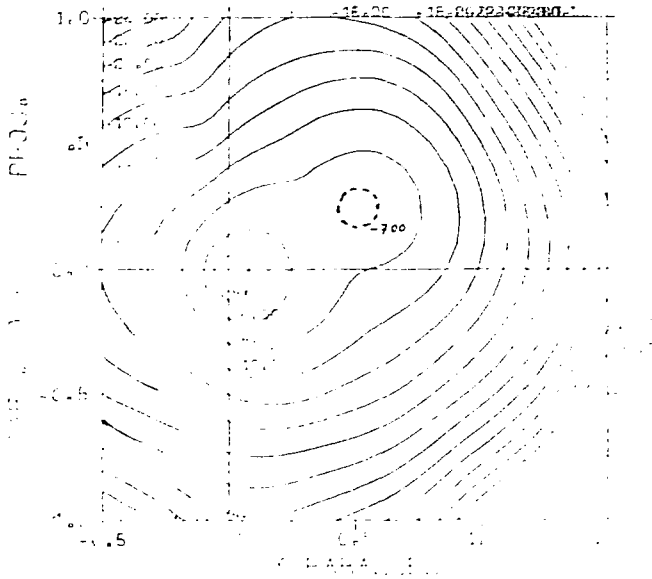


Fig. 27



1.1.2

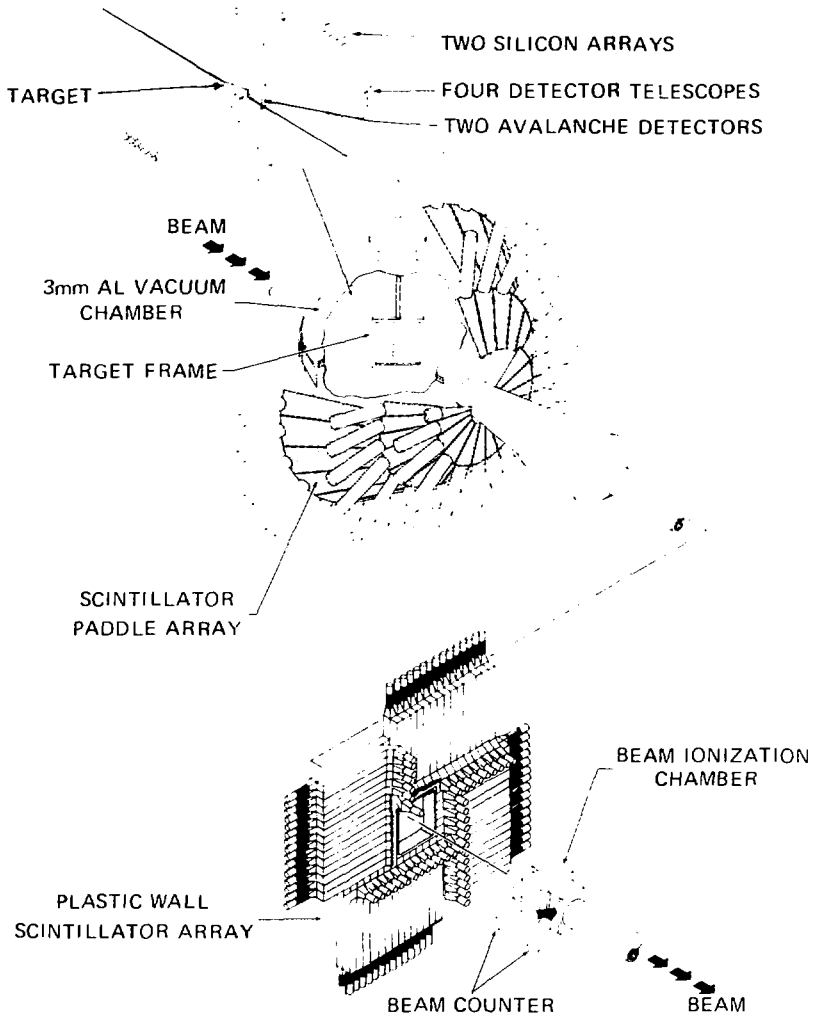


Fig. 29

XBL808-1691

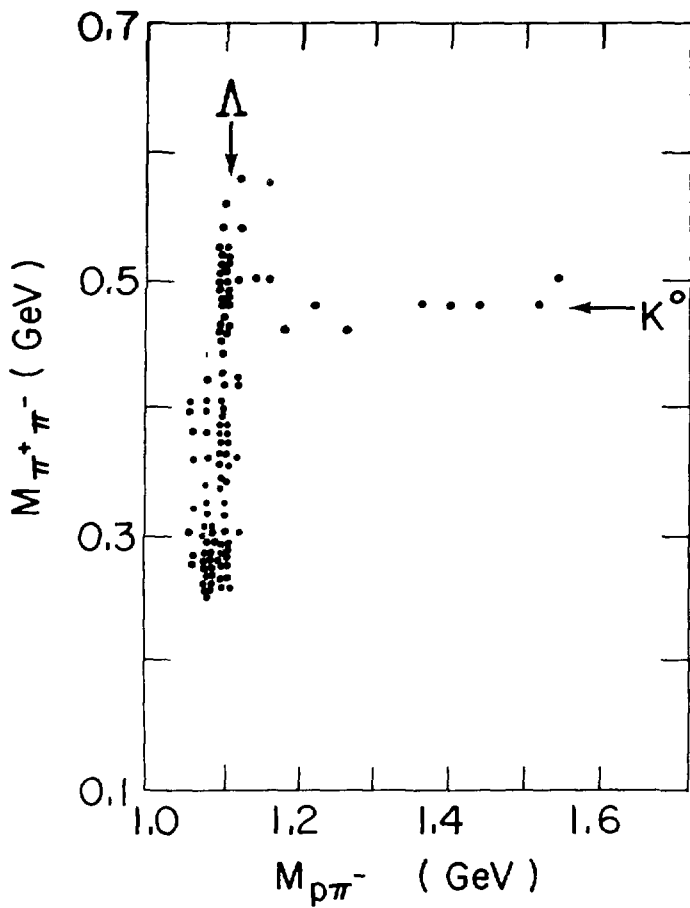


Fig. 30

XBL 804-753